Photophysical Properties and Single-Molecule Magnet Behavior in Heterobimetallic 3d4 f Schiff Base Complexes

F.Z. Chiboub Fellah, F. Pointillart, Thierry Guizouarn, T. Roisnel, N. Dege, A. Chiboub Fellah, R. Hassaine

Photophysical Properties and Single-Molecule Magnet Behavior in Heterobimetallic 3d4f Schiff Base Complexes

Fatima Zohra Chiboub Fellah*[a], Fabrice Pointillart*[b], Thierry Guizouarn[b], Thierry Roisnel[b], Necmi Dege[c], Abdelghani Chiboub Fellah[d], Ridha Hassaine[e,f]

[a] Prof F. Z. Chiboub Fellah, Laboratoire de Chimie Inorganique et Environnement, Université de Tlemcen, BP 119, 13000 Tlemcen, Algeria. E-mail: cfatema@yahoo.fr
[b] Dr. F. Pointillart, Mr. T. Guizouarn, Dr. T. Roisnel, Univ Rennes, CNRS, ISCR (Institut des Sciences Chimiques de Rennes) - UMR 6226, F-35000 Rennes, France. E-mail:fabrice.pointillart@univ-rennes1.fr
[c] Dr N. Dege, Ondokuz Mayis University, Faculty of Arts and Sciences, Department of Physics, 55200 Atakum, Samsun, Turkey.
[d] Prof A. Chiboub Fellah, Laboratoire de Valorisation des Ressources en Eau, Équipe de chimie de coordination, Université de Tlemcen, BP 119, 13000 Tlemcen, Algeria.
[e] Dr R. Hassaine, Laboratoire de Catalyse et Synthèse en Chimie Organique, Université de Tlemcen, BP 119, 13000 Tlemcen, Algeria.
[f] Dr R. Hassaine, Centre de Recherche Scientifique et Technique en Analyses Physico – ChimiquesCRAPC, Bou-Ismail BP 384, 42004 Tipaza, Algeria.

Abstract: Three new heterobimetallic Schiff base complexes of formula $[(LZnCl)_2Gd(H_2O)](ZnCl_4)_{0.5}$. (**2**), $[(LZn(OH))(LZnCl)Sm(H_2O)](ZnCl_4)_{0.5}$ (**3**) and $[(LZnCl_{0.5}(OH)_{0.5})(LZnCl)Dy(H_2O)](ZnCl_4)_{0.5}$ (**4**) were designed from the reaction of the metallo-ligand ZnL (**1**) (H_2L = N, N′-bis(3-methoxysalicylaldiimine)-1,3-propylene-2-ol) and lanthanide salt in a ratio 1 to 1. The crystallographic structures of **2**-**4** were resolved by single crystal X-ray diffraction. Light irradiation allowed the observation of a broad emission centered on the organic ligand which is exalted upon Zn(II) coordination. **1** is able to act as a metallo-organic chromophore for the sensitization of the Sm(III) luminescence. Finally the Dy(III) derivative displayed Single-Molecule Magnet (SMM) behavior with an opening of the hysteresis loop up to 5 K and a magnetic relaxation operating through Orbach, Raman and Quantum Tunneling of the Magnetization (QTM) at 0 Oe while under an applied magnetic field the QTM is efficiently cancelled.

Introduction

Lanthanide elements are ~~at~~ the center of interest in the molecular magnetism field since the discovery of slow magnetic relaxation for a mononuclear complexes in 2003. Such magnetic behavior can lead to the observation of magnetic bistability at low temperature and potential applications in high-density data storage [1], and spintronic devices [2]. The required strong magnetic anisotropy is obtained ~~thank to~~ by the optimization of the coordination environment (crystal field) for obtaining a large splitting of the ground multiplet state. Following this strategy, Single-Molecule Magnet (SMM) with blocking temperature up to 80 K was designed[3]. Then additional strategies were applied to cancel the under-barrier magnetic relaxation processes such as the Quantum Tunnelling of the Magnetization (QTM) and Raman process due to the presence of dipolar and hyperfine interactions. These strategies consist in isotopic enrichment [4], modification of the molecular vibrations [5], and magnetic dilution through frozen solution [6], doping in diamagnetic matrix [7] and inclusion of diamagnetic transition metal [8] [9] [10].

Otherwise, the development of new luminescent materials, based on rare-earth ions, is a highly competitive research topic, due to the many applications to which these materials can lead. This enthusiasm was sparked by the emergence of new technologies such as energy-saving lighting sources, large display screens, fluorescent markers, responsive luminescent stains for biomedical analysis, and medical diagnosis [11].

Indeed, the majority of trivalent ions are very strongly fluorescent when subjected to excitation, the return to the ground state is accompanied by the emission of radiation in the form of a fine line, leading to a high purity of color. The luminescence properties of Ln ions are derived from intra-configurational ($4f^n \rightarrow 4f^n$) and inter-configurational ($4f^{n-1}5d^1 \rightarrow 4f^n$) electronic transitions. The long lifetimes of the excited state is due to the Laporte-forbidden[12] character of the f-f transitions but it induced weak absorption coefficient making sensitization emission poorly achievable by direct excitation. Thus a more efficient sensitization can be reached by indirect energy/electron transfer for an organic ligand acting as antennae and generally referred as an antenna effect through triplet excited-state sensitization processes, induced triplet metal-ligand charge transfer (MLCT) or singlet excited-state pathways with intra-ligand charge transfer (ILCT)[13].

In this work, we are interested in the Schiff base hetero-metallic complexes which are very captivating in recent years. Depending on the intended application and area of interest, their formulas and structures change[14]. The most common are those formed with 3d and 4f ions, in this category, a dinuclear are the most explored [15]. When the nuclearity increases, tri, tetra ... nuclear (poly-nuclear), these compounds become rarer which makes them even more attractive.[16] All these complexes exhibit a particular activity because of their structural and magneto-optical properties, particularly the physicochemical characteristics of the lanthanide ions (significant spin values, magnetic anisotropy, emitting properties) which have opened many possibilities to the design of multifunctional compounds.

The optimization of the luminescent properties is mainly based on the interactions between 4f ions and their environment and therefore depends on the material into which they will be inserted and also the method of synthesis adopted [17], although in our case, the 4f-4f emissions are the most preferred.

In this study, we carried out three ZnLnZn tri-nuclear complexes (**2**, **3**, and **4**) obtained from a lanthanide salt (Ln(III) = Gd, Sm, Dy) and a Zn precursor complex formed from zinc acetate and ligand H2L: N, N′-bis(3-methoxysalicylaldiimine)-1,3-propylene-2-ol

(Figure 1). Their single crystal X-ray diffraction structures, photophysical and magnetic properties were investigated.

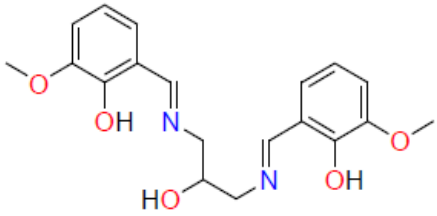

Figure 1. Ligand N, N′-bis(3-methoxysalicyl aldiimine)-1,3-propylene-2-ol (H_2L)

Table 1. Crystal data and structure refinement for **2, 3** and **4**.

Formula	2($C_{38}H_{42}Cl_2GdN_4O_{11}Zn_2$)$ZnCl_4$ (**2**)	2($C_{38}H_{43}ClN_4O_{12}SmZn_2$),$ZnCl_4$ (**3**)	2($C_{38}H_{42.5}Cl_{1.5}DyN_4O_{11.5}Zn_2$),$ZnCl_4$ (**4**)
Fw(g/mol)	2386.57	2335.90	2378.51
Crystal system	orthorhombic	orthorhombic	orthorhombic
Space group	'P b c n'	'P b c n'	'P b c n'
a [Å]	26.8928(7)	28.088(2)	27.929(2)
b [Å]	22.2552(7)	22.685(2)	22.688(2)
c [Å]	16.2366(4)	15.750(2)	15.6842(8)
λ[Å]	0.71073	0.71073	0.71073
V/ [Å^3]	9717.7(4)	10035.9(2)	9938.6(1)
d/[g/cm^3]	1.631	1.546	1.590
Z	4	4	4
T [K]	296	150	150
F(000)	4744	4664.0	4728
μ, mm^{-1}	2.845	2.552	2.925
θ rang, deg	1.514 - 26.000	2.646 - 27.463	2.216 - 27.526
Reflns meads	60871	11291	11376
Reflns used	9550	6934	7557
parameters	552	560	558
R_{int}, R1[a], wR2[a] [I>2σ-I)]	0.0599, 0.0466, 0.1082	0.0670, 0.0508, 0.1200	0.0710, 0.0549, 0.1177

[a] R1 = Σ|F_o| – |F_c|Σ|F_o|. wR2 = [Σw[(Fo^2– Fc^2)^2]/Σ|[w(Fo^2)^2]]$^{1/2}$. w=1/[$σ^2$(Fo^2)+(0.075P)^2], where P = [max(Fo^2,0)+2Fc^2]/3

Results and Discussion

1. Synthesis analysis

What differs our compounds from tri-nuclear complexes already known all resulting from a ratio LZn / lanthanide salt (2/1) [9a, 10, 18], ours are obtained from a single equivalent of precursor complex (LZn) and a single equivalent of the lanthanide salt at room temperature and without adding anything. Complex **2**, ZnGdZn was made first, from one equivalent of LZn and one equivalent of gadolinium chloride salt, the replacement of lanthanide chlorides by nitrates gave us dinuclear ZnLn or tetranuclear Zn2Ln2 compounds already known in the literature[15b, 17b, 19]. Finally, we tried to use lanthanide nitrates but in the presence of $ZnCl_2$, ~~always~~ still with an LZn / lanthanide nitrate / $ZnCl_2$ ratio (1/1/1), and here again we produced trinuclear for complexes **3** and **4**. Chloride ions from $ZnCl_2$ certainly replaced the nitrate ions from the lanthanide salt since they are much more soluble, but without binding to the lanthanide cation. A priori, the lanthanide does not like to bind to chloride in this type of trinuclear, as with the nitrate ions [20], preferring to transfer it to the 3d cation while attracting other ligands towards it, [21], even if the two metals (Zn and Ln) are chloride salts[9a, 21b]. This difference in design can be explained mainly by the synthesis conditions adopted. The ligand used is characterized by the presence of the hydroxy function of the diamine, the oxygen ~~of which does~~ not bind with the 3d metal, as is the case with some complexes [22], ~~but it~~ is involved in general, through its H in hydrogen bonds between different units and the formed counter anion $[ZnCl_4]^{2-}$. With this arrangement of OH, few studies are known with this ligand [17b, 23]. Recently, ZnLnZn tri-nuclear resulting from lanthanide nitrate with an LZn/nitrate-Ln ratio of (2/1) have been published [24].

2. X-ray structure analysis

X-ray structure of 2. Complex **2** has ~~a~~ the following formula: $[(LZnCl)_2Gd(H_2O)](ZnCl_4)_{0.5}$. It crystallizes in the orthorhombic space group Pbcn. A perspective view of this trinuclear molecule, is shown in Figure 2 and the significant bond lengths and angles, are listed in the caption. The asymmetric unit is formed ~~of~~ by a cationic trinuclear entity and a half of the counter-anion $[ZnCl_4]^{2-}$ to ensure neutrality.

The central core of the molecule consists of three metal ions, two zinc ions separated by gadolinium, which is slightly closer to Zn2 than to Zn1 with bond lengths of 3.537(8) and 3.648(9) Å respectively, whereas the distance between the two Zn is 7.166(1) Å. The shortest intermolecular Gd–Gd distance ~~is~~ equals to 9.9387(6) Å. The three ions Zn1, Gd1, and Zn2 are practically aligned, with Zn1···Gd1···Zn2 angles 171.473(3)°. The gadolinium is nine coordinated with one oxygen (O11) in the axial position from the water molecule [Gd1–O11, 2.443(4) Å] and four oxygen from each ligand, two from the bridging phenolic groups and two from the methoxy groups, Gd1–Oi (i=2…9) bond lengths range from 2.335(4) to 2.630(4) Å. The Gd(III) coordination polyhedron was determined as a distorted spherical tricapped

trigonal prism with a D_{3h} symmetry with SHAPE analysis[25] (1.943, CShM JTCTPR-9, Table S1).

The zinc ions are in a square pyramidal environment. In fact, in addition to the chloride ion in the axial position, two nitrogen and two oxygen atoms from the ligand (N1N2O3O4) and (N3N4O7O8) surround each zinc (Zn1 and Zn2), which are slightly detached from these mean equatorials plans towards chloride ions by a distance of -0.560(1) and 0.599(1) Á. The chloride ion Cl2 attached to Zn2 is in the same direction as the oxygen O11 attached to gadolinium, while the Cl1 attached to Zn1 is in the opposite direction. The bound lengths Zn1–Cl1 and Zn2–Cl2 2.282(2) and 2.271(2) Á are homogeneous and shorter than that of Gd1–O11. Given the structure of the ligand, several hydrogen bonds are involved but three of them are distinguished. There is a moderate intramolecular bond O11-H11D···Cl2 between the oxygen of the water molecule attached to gadolinium and the Cl2 attached to the Zn2 ion.

Two other very weak intermolecular hydrogen bonding ensures the cohesion of the crystal, forming a 1D chain of trinuclear units (Figure S2). The first one is between the hydroxyl oxygen of the diamine O1 (in the axial position of the six-member ring formed by the diamino moiety and the Zn atom) and the chloride Cl4 of the counter anion $[ZnCl_4]^{2-}$. The second one, which is even weaker, is involved between the hydroxyl of a diamine of the second ligand O10, always in the axial position, and the chloride Cl3 of another counter anion. In both cases, this OH unit acts as an H-bond donor group.

Figure 2. Molecular structure of $[(LZnCl)_2Gd(H_2O)](ZnCl_4)_{0.5}$ (**2**). The thermal ellipsoids are drawn at the 30% probability level. Selected bond lengths (Á) and angles (°) : Gd1–O2 2.594(4), Gd1–O3 2.346(3), Gd1–O4 2.336(4), Gd1–O5 2.630(4), Gd1–O6 2.513(4), Gd1–O7 2.343(4), Gd1–O8 2.342(4), Gd1–O9

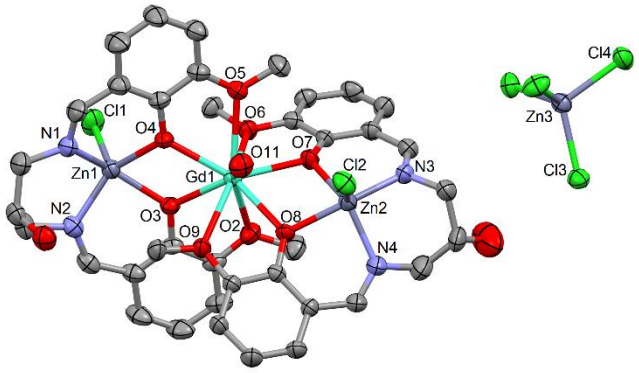

2.582(4), Gd1–O11 2.443(4), Zn2–N3 2.015(6), Zn2–O8 2.042(4), Zn2–N4 2.056(5), Zn2–O7 2.098(4), Zn2–Cl2 2.271 (2), Zn1–N2 2.051(5), Zn1–O4 2.083(4), Zn1–O3 2.095(4), Zn1–N1 2.096(6), Zn1–Cl1 2.282(2), Gd1···Zn1 3.648(9), Gd1···Zn2 3.537(8), Zn1···Zn2 7.166(1), Zn3–Cl4 2.255(2), Zn3–Cl3 2.274(2). Zn1–O3–Gd1 110.3(2), Zn1–O4–Gd1 111.2(2), O3–Zn1–O4 73.7(2), O3–Gd1–O4 64.7(2), O7–Zn2–O8 75.4(2), O7–Gd1–O8 65.4(2), Zn2–O7–Gd1 105.5(2), Zn2–O8–Gd1 107.4(2),O2–Gd1–O5 141.7(2), O6–Gd1–O9 153.8(2), O2–Gd1–O9 85.5(2), O5–Gd1–O6 69.6(2).

X-ray structure of 3. The asymmetric unit of complex **3** is formed of the cation $[(LZnCl)Sm(H_2O)(LZn(OH))]^+$ and a half counter anion $ZnCl_4^{2-}$. The three metallic centers are more aligned than in complex **2**, with a ZnSmZn angle equal to 174.896(2)°. The structure of the complex with the relevant values of the angles and bond lengths are shown in Figure S3. The two entities each comprising a Zn^{2+} cation form a site into which the Sm^{3+} cation is inserted. The latter is surrounded by nine oxygens, identical in positions ~~identical~~ to those of complex **2**. The Sm(III) coordination polyhedron can be determined as a spherical capped square antiprism with a C_{4v} symmetry (2.025, CShM CSAPR-9), a distorted spherical tricapped trigonal prism with a D_{3h} symmetry (2.127, CShM JTCTPR-9) or a Muffin with Cs symmetry (2.284, CShM MFF-9) (Table S1). The distances between the Sm^{3+} cation and the $Zn1^{2+}$ and $Zn2^{2+}$ cations are respectively 3.596(6) and 3.674(6) Å with a separation between the two Zn cations of 7.263(7) Å. Each Zn cation has five near neighbors, two imino nitrogen atoms, and two phenolato oxygen atoms in the equatorial positions, those apical are occupied by a chloride anion for $Zn1^{2+}$ and oxygen coming from a hydroxide anion for $Zn2^{2+}$. This terminal bond with a Zn-O length of 2.197(4) Å is more elongated than its equivalents in apical position, which have the same square-based pyramid geometry of the ZnII metal center. This is valid whether it is terminal as for the Zn-O bond lengths of the two enantiomers of the Zn2Dy [21b] complex which vary between 2.021(4) and 2.046(4), or non-terminal as the trinuclear Zn2Ln Schiff base complexes with Zn-O lengths ranging from 1.988(5) to 2.009(6) Å [24], in this case the zinc is bonded to a peroxo oxygen which forms with the second oxygen a bridge between the Zn(II) and Ln(III). Each zinc cation is linked to Sm by two phenolato bridges. The dihedral angle between the two planes containing Zn and Sm, Zn1O19SmO34, and Zn2O49SmO64 is equal to 70.983(2)°. The hydrogen bonds in this complex are very weak and are only intramolecular~~. They are~~ shown in Figure S3.

X-ray structure of 4. The structure of complex **4** is the same as ~~that~~ of complex **3**, except that the apical bond of the $Zn2^{2+}$ cation is shared 50/50 between the hydroxide anion OH^- and the chloride anion Cl^-. Thus the Dy(III) coordination sphere can be also described with the three spherical capped square antiprism (1.736, CShM CSAPR-9), spherical tricapped trigonal prism (1.826, CShM JTCTPR-9) and Muffin (2.003, CShM MFF-9) (Table S1). Even this complex is near-linear, the angle between the three metallic centers ~~is~~ equals to 174.626(3)°. A single intra-molecular hydrogen bond is formed between the Cl1 bound to Zn1 and the O1 of the H_2O molecule bound to Dy. Each two asymmetric Zn2Dy units are linked through the anion $ZnCl_4^{2-}$ which bridges the two, to form with each unit, an intermolecular hydrogen bond through its chlorine Cl11 and the oxygen O54 of the hydroxy group of the diamine of the ligand. The structure with its hydrogen bonds is shown in Figure S4.

2 Emission Properties

The emission spectra of the free ligand, complex **1**, and heterobimetallic complexes **2**-**4** were carried out at room temperature in MeOH solution, and are represented in the Figure 3. Excitation at 346 nm of the free ligand led to a centered ligand emission localized at 477 nm (Figure 3).

Upon coordination of the diamagnetic Zn(II) ion and under irradiation at 366 nm (see Figure S5 for absorption spectra), the ligand emission is exalted. Under the excitation of 366 nm, this band appears at 449 nm in the case of **2** without the appearance of any other peak [26]. What was expected for this complex as Gd^{3+} with a half filled $4f^7$ type configuration which shows 4f-4f type transitions in the UV range. Under an excitation of 350 nm, this same band is much less intense in complex **4** and appears at 455 nm. Another weak band appears at 574 nm, corresponding to the emission between the energy levels $^4F_{9/2}$ and $^6H_{13/2}$ (inset of Figure 3). This transition is purely electric dipole (DE) in nature[15a,

[27]. In other words, a dual emission of the free ligand and the Dy(III) ion was observed. Finally, the emission spectrum of **3** recorded under 370 nm excitation is shown in Figure 3. A residual emission of the organic ligand was observed at 453nm, which is much less intense compared to the other two complexes (Gd, Dy), together with the classical visible Sm(III) centered emission spectrum. These bands located at values of λ = 563, 596, 644, and 714 nm are due respectively to the transitions from the transmitter level $4G_{5/2}$ to the ground state multiplets $6H_J$ (J = 5/2, 7/2, 9/2, and 11/2). The most intense transition $4G_{5/2} \rightarrow 6H_{7/2}$ located around 596 nm is of a magnetic dipole (DM) nature, authorized since ΔJ = ± 1. This transition splits into two peaks: 596 nm and the least intense is at 608 nm. The transition $4G_{5/2} \rightarrow 6H_{9/2}$, with a hypersensitivity property (ΔJ = 2), of electric dipolar nature (DE) is much more intense than that of $4G_{5/2} \rightarrow 6H_{5/2}$ (DM) specifying the asymmetric nature of the environment of the Sm^{3+} ions [26b]. The asymmetric character indicates that the Sm^{3+} ions do not occupy any site with inversion symmetry. A weak peak is observed at about 714 nm and is attributed to the $4G_{5/2} \rightarrow 6H_{11/2}$ transition, the latter is not present in all complexes of this type[28].

Figure 3. Emission spectra in MeOH (c = 2.10^{-5} M) of the free ligand (λ_{ex}= 346nm, black line), complexes **1** (λ_{ex} = 370nm, green line), **2** (λ_{ex} = 366 nm, blue line), **3** (λ_{ex} = 370 nm, purple line) and **4** (λ_{ex} = 350nm, red line). In inset: zoom on emission of complex **4**.

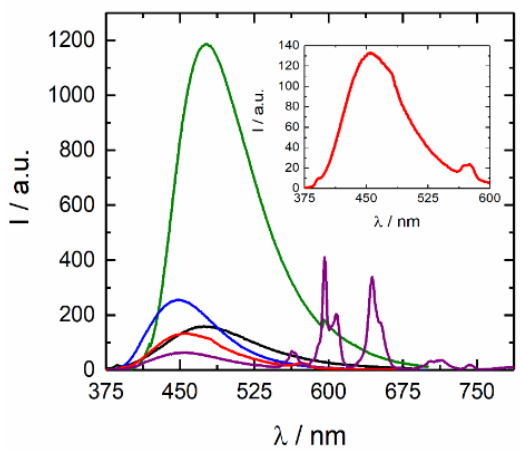

3 Magnetic Properties

The $\chi_M T$ temperature dependences for the complexes **2** and **4** are reported in Figure S6. The room temperature values are 7.84 cm^3 K mol^{-1} and 13.30 cm^3 K mol^{-1} for the Gd(III) and Dy(III) complexes respectively in agreement and slightly lower than the theoretical expected values of 7.875 cm^3 K mol^{-1} and 14.17 cm^3 K mol^{-1} for one isolated Gd(III) (8S ground state multiplet) and Dy(III) ($^6H_{15/2}$ ground state multiplet), respectively [29] On cooling down at 2 K the $\chi_M T$ values decrease monotonically to 7.34 cm^3 K mol^{-1} for **2** and 10.47 cm^3 K mol^{-1} for **4** (Figure S6). The Curie law deviations can be mainly explained by the thermal depopulation of the M_J states (for **4**) and possible dipolar antiferromagnetic interactions at very low temperature (for **2**). The inset of Figure S6 depicted the field dependences of the magnetization measured at 2 K. The values reached under a magnetic field of 50 kOe are 6.9 Nβ and 4.9 Nβ for **2** and **4**. These values are in line with the expected saturation value for an isotropic Gd(III) ions but far from the expected one of 10 Nβ for an isolated Dy(III) indication of significant magnetic anisotropy.

In view of the dc magnetic properties, the Dy(III) derivative was investigated by ac magnetic measurements. **4** exhibits slow relaxation of the magnetization in zero applied field (Figures 4a and S7). The normalized Argand plot for **4** indicates that the observed slow magnetization relaxation represents more than 90% of the signal detected in the static measurements (Figure S8). The extended Debye model (SI and Table S2) can be used to fit the dynamic data and allow the extraction of the relaxation times (τ). The resulting thermal dependence of τ could be fitted (Equation 1) with a combination of QTM, Raman and Orbach (Figure S9) processes by using τ_{TI} = 1.91(4)×10^{-3} s, C = 0.11(5) s^{-1} K^{-n} with n = 3.4(2), τ_0 = 2.57(1)×10^{-9} s and Δ = 250(9) K (Figure 4d).

$$\tau^{-1} = \underbrace{\tau_0^{-1}\exp\left(\frac{\Delta}{T}\right)}_{Orbach} + \underbrace{CT^n}_{Raman} + \underbrace{\frac{B_1}{1+B_2H^2}}_{\tau_{TI}^{-1},QTM} + \underbrace{ATH^m}_{Direct} \qquad \text{Eq. 1}$$

In the case of a pure acoustic phonons (lattice vibrations) Raman process, the expected n value is 9 for Kramers ions [30] but the involvement of optical phonons (molecular vibrations) [3] can induce the diminution of n between 2 and 7 [5a, 31] [32].

Under a static magnetic field (Figures S10), the out-of-phase maxima start to move to lower frequencies. Two contributions can be distinguished for the low magnetic field values usually attributed to the presence of dipolar magnetic interactions between the Dy(III) magnetic centers[33]. By applying field values higher than 400 Oe only one contribution is observed. The relaxation times are extracted from the field dependence of the χ_M curves (Figures S11 and 4c) (Table S3). The field dependence of the extracted τ can be fit by Equation 2 (Figure 4b)[34],[35].

$$\tau^{-1} = \frac{B_1}{1+B_2H^2} + 2B_3H^4 + k(T) \qquad \text{Eq. 2}$$

The fit parameters are B_1 = 1.1(1)×10^{45} s^{-1}, B_2 = 1.6(4)×10^{40} Oe^{-2}, B_3 = 1.4(7)×10^{-15} s^{-1} K^{-1} Oe^{-4} and k(T) = 4(1)×10^{-1} s^{-1}. The optimal value of 1200 Oe was selected to study the in-field temperature dependent behavior of **4** (Figure 4b). As already observed under zero applied magnetic field, the normalized Argand plot for **4** indicates that the observed slow magnetization relaxation under an applied magnetic field represents approximately all the signal detected in the static measurements (Figure S12). The data for **4** can be interpreted with an extended Debye model (Table S4) and the best fit of the log(τ) vs T curve (Figure 4d) was obtained using a combination of Orbach (fixed to the parameters found for **4** in zero applied magnetic field) (τ_0 = 2.57×10^{-9} s and Δ = 250 K) and Raman (C = 3.86(3) ×10^{-5} s^{-1} K^{-n} with n = 5.87(4)) processes while the QTM was cancelled by the 1200 Oe applied field. The fit parameters are B_1 = 1.1(1)×10^{45} s^{-1}, B_2 = 1.6(4)×10^{40} Oe^{-2}, B_3 = 1.4(7)×10^{-15} s^{-1} K^{-1} Oe^{-4} and k(T) = 4(1)×10^{-1} s^{-1}. The optimal value of 1200 Oe was selected to study the in-field temperature dependent behavior of **4** (Figure 4b). As already observed under zero applied magnetic field, the normalized Argand plot for **4** indicates that the observed slow magnetization relaxation under an applied magnetic field represents approximately all the signal detected in the static measurements (Figure S12).

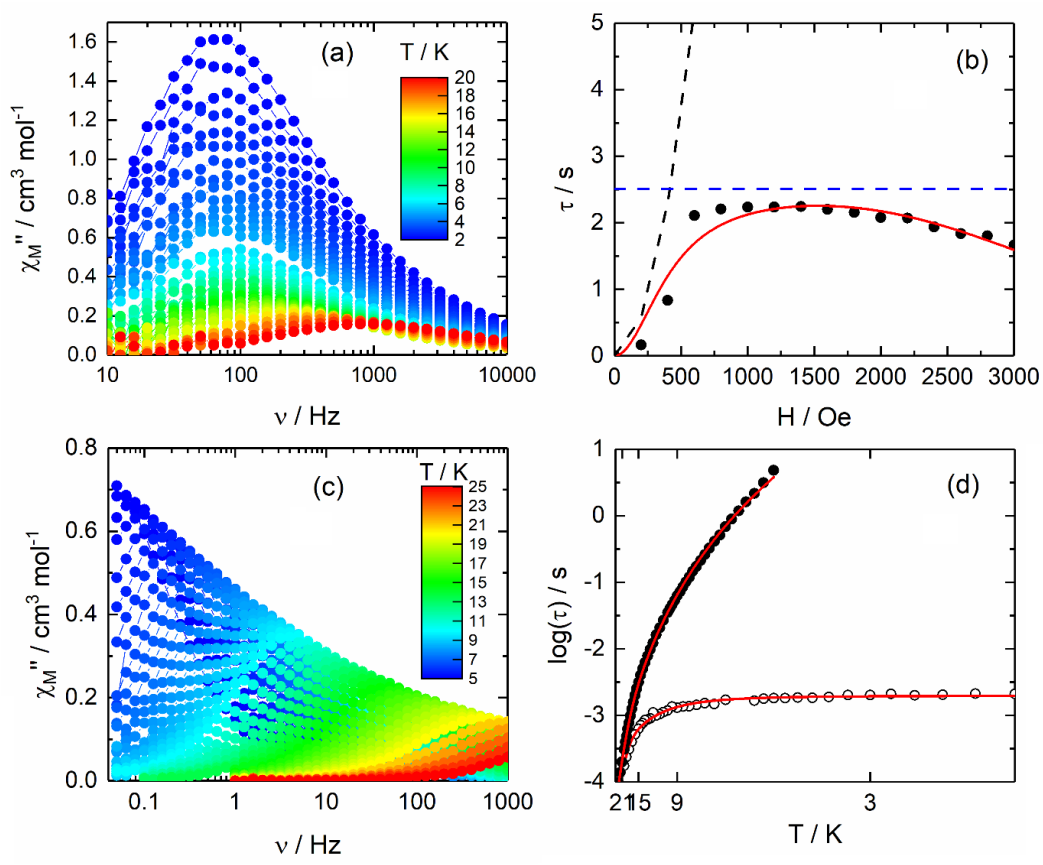

Figure 4. (a) Frequency dependence of χ_M'' at zero applied magnetic field for **4** in the temperature range 2-20 K. (b) Field dependence of the relaxation time at 2 K for **4** with representation of the best fit curve (full red line) and the QTM (black dashed line) and thermally activated (blue dashed line) contributions (the direct contribution is not visible in the selected scale). (c) Frequency dependence of χ_M'' at 1200 Oe applied magnetic field for **4** in the temperature range 5-25 K. (d) Temperature variation of the relaxation time for **4** in zero (open circles, temperature range 2-20 K) and 1200 Oe (full circles, temperature range 5-25 K) applied magnetic field. The best fits (full red lines) are obtained with parameters given in the text.

The data for **4** can be interpreted with an extended Debye model (Table S4) and the best fit of the log(τ) vs T curve (Figure 4d) was obtained using a combination of Orbach (fixed to the parameters found for **4** in zero applied magnetic field) ($\tau_0 = 2.57\times10^{-9}$ s and Δ = 250 K) and Raman (C = 3.86(3) $\times10^{-5}$ s^{-1} K^{-n} with n = 5.87(4)) processes while the QTM was cancelled by the 1200 Oe applied field. Such magnetic relaxation processes and dynamic parameters are in line with those previously observed for similar trinuclear Zn-Dy-Zn complexes in which the Dy(III) is coordinated to nine oxygen atoms[10]. Indeed, a quick survey of the literature highlighted an effective energy barrier for the reversal of the magnetization which ranges from 96.7 K to 233 K for a Dy(III) in O9 environment with the ninth oxygen atom is H_2O[19b],[10] or MeOH.[10] The replacement of the latter with Cl^- or O^- (coming from a bridging acetate) anion led to an increase of U_{eff} = 398K-481 K[10] or decrease of U_{eff} = 22.4 K[36];respectively.

The hysteresis loops were measured in the temperature range of 2-5 K (Figure 5). As predicted by ac results, the hysteresis is close at 0 Oe due to the efficient QTM and opens for H > 400 Oe when the thermally activated relaxations started to be the main processes (Figure 4b) and finally closes at high field when direct process is operating. At the end a classical butterfly shaped hysteresis was observed up to 4 K as commonly observed for mononuclear Dy^{3+} SMMs.[37]

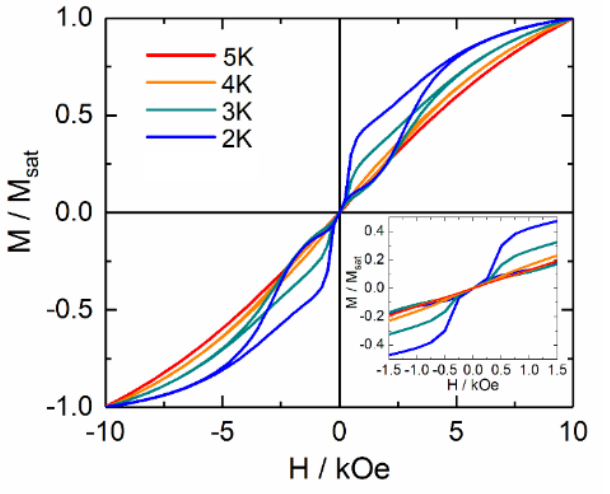

Figure 5. Normalized magnetic hysteresis loops between 2 and 5 K at a sweep rate of 16 Oe s^{-1} for 4. The inset corresponds to a zoomed view of the origin.

Conclusions

In this paper, three new heterobimetallic Schiff base complexes were obtained as single crystals by the equimolar reaction of ZnL (**1**) (H2L= N, N′-bis(3-methoxysalicylaldiimine)-1,3-propylene-2-ol) and lanthanide salt. The crystallographic structures of $[(LZnCl)_2Gd(H_2O)](ZnCl_4)_{0.5}$. (**2**), $[(LZn(OH))(LZnCl)Sm(H_2O)](ZnCl_4)_{0.5}$ (**3**) and $[(LZnCl_{0.5}(OH)_{0.5})(LZnCl)Dy(H_2O)](ZnCl_4)_{0.5}$ (**4**) revealed the formation of Zn2Ln trinuclear Schiff base complexes in which the two Zn(II) have a pyramidal geometry with a square base linked by a lanthanide ion surrounded by nine oxygen atoms.

The coordination of the Zn(II) ion enhanced the broad emission of the L^{2-} ligand. The resulting metallo-ligand (**1**) played the role of chromophore for the sensitization of the Sm(III) luminescence while an efficient back energy transfer led to a poor sensitization in case of the Dy(III) ion.

The ac magnetic measurements revealed the SMM behavior for **4** with a magnetic relaxation occurring through a combination of Orbach, Raman and QTM in zero applied magnetic field. The later can be cancelled by applying a 1200 Oe magnetic field and a magnetic bistability can be observed up to 5 K.

Experimental Section

Physical measurements

Elemental analysis for C, H, and N was carried out using a Perkin-Elmer 240C elemental analyzer and at the Centre Régional de Mesures Physiques de l'Ouest, Rennes. IR spectra were recorded in the range of 4000–400 cm^{-1} on a Perkin Elmer FT-IR spectrophotometer using a KBr pellet. The absorbance of complexes was measured using Lambda 25 Perkin Elmer UV-Vis spectrometer. Measurements of ^1H NMR spectra were conducted using a Bruker Avance 400WB spectrometer in DMSO-d6, at ambient temperature (295 K). Emission was examined by Shimadzu RF 6000 spectrofluorimeter at room temperature (295 K) in methanol solution ($2\cdot10^{-5}$ M). Single crystal of complexes were mounted on a STOE IPDS II diffractometer for data collection (MoK_α radiation source, λ = 0.71073 Å) at room temperature (for **2**) from Ondokuz Mayis University and on a APEXII Bruker-AXS diffractometer (MoK_α radiation source, λ = 0.71073 Å) 150 K (for **3** and **4**), from the Diffractometric Centre X (CDIFX), University of Rennes 1, France (Table 1). The SHELXT program[38] was used to solve the structures with a direct method and refinements were done with the SHELXL-14/7 program[39] using a full matrix least-squares method on F2. The CCDC number are: 1877440, 2174946 and 2174947, for compounds **2,** **3**, and **4,** respectively. The static susceptibility measurements were performed on solid polycrystalline samples with a Quantum Design MPMS-XL SQUID magnetometer. The following values of magnetic field were used 0.2 kOe, 2 kOe and 10 kOe respectively for the temperature range of 2-20 K, 20-80 K and 80-300 K in order to prevent any saturation effect. The ac magnetic susceptibility measurements were performed on both Quantum Design MPMS-XL SQUID magnetometer (1-1000 Hz frequency range) and Quantum Design PPMS 14 T magnetometer (10-10000 Hz frequency range). Immobilized selected and crunched single crystals were employed to realize the magnetic measurements and the latter were all corrected for the diamagnetic contribution as calculated with Pascal's constants.

Synthesis

Materials: All chemicals, obtained from Aldrich, were of reagent grade and were used for the syntheses without further purification. High-grade solvents (acetone, methanol) and distilled water were used for the preparation of the complexes.

Preparation of [LZn(H2O)] (1). To a stirred solution of orthovanilin (0.304 g, 2.0 mmol) and 1,3-diamino-2-propanol (0.09 g, 1.0 mmol) in 10 ml of absolute methanol was first added an excess of triethylamine (0.303 g, 3.0 mmol). After stirring for 30 min, Zinc Acetate (0.219 g, 1.0 mmol) dissolved in acetone (10 ml) was added at once with stirring at room temperature. Two hours later, the yellow precipitate was filtered off, washed with cold methanol, and diethyl ether. Yield: (382.36 mg, 87%). Elemental analyses were used to characterize the starting material. Analysis Calc. for $C_{19}H_{20}ZnN_2O_5.H_2O$, C, 51.77; H, 4.53; N, 6.20; found C, 51.89; H, 5.04; N, 6.37.IR (cm^{-1}, KBr): 3525(m); 3332(m); 3055(w);2930(w); 1627(s); 1605(w); 1551(w); 1450(s); 1325(m); 1244(m); 1228(s);1120(w); 1054(w); 1010(m); 954(m); 853(w); 725(w); 630(s). 1H NMR (DMSO-d6) δ: 3.53 (m, 2H); 3.71 (s, 6H); 3.86 (d, 2H); 4.04 (q, 1H); 5.19 (d, 1H); 6.32 (t, 2H); 6.76 (m, 4H); 8.20 (s, 2H). UV–vis (295K, λ max (nm)): 228, 271, 359.

Preparation of $[(LZnCl)_2Gd(H_2O)](ZnCl_4)_{0.5}$. (2). The heterotrinuclear compound Zn–Gd–Zn was prepared as follows: To the Schiff base complex ZnL (0.2 mmol, 0.085g) dissolved in 10 mL of acetone, produces a yellow colored solution, was added slowly the freshly prepared solution of $GdCl_3.6H_2O$ (0.2 mmol, 0.075g) in 10 mL of methanol. The resulting deep yellow solution was stirred for 1hour. The solution obtained was left undisturbed. Crystals of the desired compound were obtained over ten days. This technique yielded crystals suitable for X-ray diffraction studies. Yield: (0.127 g, 52,4%). Elemental analyses were used to characterize the starting material. Analysis Calc. for $C_{38}H_{42}Cl_4GdN_4O_{11}Zn_{2.5}$ (1193.23g mol^{-1}): C, 38.22; H, 3.52; N, 4.69; found C, 38.41; H, 3.71; N, 4.62. IR (cm^{-1}, KBr): 3428(s); 1629(s); 1608 (w); 1562(w); 1474(m); 1411(w); 1384(s); 1286(m); 1243(w); 1223(s); 1056(w); 949(m); 848(w); 741(m);597(w). UV–vis (295K, λ_{max} (nm)): 220, 266, 346.

Preparation of $[(LZn(OH))[(LZnCl)Sm(H_2O)]$ $(ZnCl_4)_{0.5}$ (3). The replacement of $GdCl_3.6H_2O$ by the mixture of $Sm(NO_3)_3.6H_2O$ and $ZnCl_2$ in a 1/1 ratio according to the same experimental process to **2** gave colourless crystals suitable for X-ray analysis after two weeks. A mixture of $Sm(NO_3)_3(H_2O)_6$ (0.2 mmol, 0.089 g) and $ZnCl_2$ (0.2 mmol, 0.027g) dissolved in 10 ml of MeOH was added to the Zn complex (0.2 mmol, 0.085g) already dissolved in 10 ml of acetone. The mixture remains under stirring for 1 hour at the end of which a homogeneous solution is obtained which will be left to crystallize in air. Yield: (0.120 g , 51,37%). Anal. calc. For $C_{38}H_{43}Cl_3SmN_4O_{12}Zn_{2.5}$ (1167.88g mol^{-1}): C, 39.04; H, 3.68; N, 4.79; found C, 39.11; H, 3.74; N, 4.70. IR (cm^{-1}, KBR): 3407 (s); 2943 (w); 1629 (s); 1609 (w); 1562 (w); 1473 (s); 1384 (s); 1286 (m); 1223 (s); 1102 (w); 1056 (m); 948 (m); 847 (m); 741 (m); 631 (w). UV–vis (295K, λ_{max} (nm)): 217, 265, 345.

Preparation of $[(LZnCl_{0.5}(OH)_{0.5})(LZnCl)Dy$ $(H_2O)](ZnCl_4)_{0.5}$ (4). Complex **4** was obtained following a procedure similar to that used to achieve complexes **3**. Yield: (0.147 g, 61%). Anal. calc. For $C_{38}H_{42.5}Cl_{3.5}DyN_4O_{11.5}Zn_{2.5}$ (1189.25 g mol^{-1}): C, 38.34; H, 3.57; N, 4.71; found C, 38.39; H, 3.66; N, 4.61. IR (cm-1, KBR): 3428 (s); 2925 (w); 1629 (s); 1608 (w); 1526 (w); 1474 (m); 1384 (s); 1286 (m); 1243 (w); 1223 (m); 1074 (w); 949 (m); 848 (m); 741 (m); 597 (w). UV–vis (295K, λ_{max} (nm)): 204, 225, 268, 348.

Acknowledgements

This work was supported by CNRS, Université de Rennes 1, and the European Commission through the ERC-CoG 725184 MULTIPROSMM (project No. 725184). This work is part of the PRFU project number B00L01UN130120180008, Fatima CHIBOUB thanks the MESRS of Algeria for awarding the project and also thanks ~~le~~ the Laboratoire de Chimie de Coordination, Toulouse, France for the analyzes of complex 1.

Keywords:

Antenna Effect, Schiff base complexes, Lanthanide, Luminescence properties, Single-Molecule Magnet (SMM).

References

[1] D. Gatteschi, R. Sessoli, J. Villain, *Molecular nanomagnets, Vol. 5*, Oxford University Press on Demand, **2006**.

[2] S. Thiele, F. Balestro, R. Ballou, S. Klyatskaya, M. Ruben, W. Wernsdorfer, *Science* **2014**, *344*, 1135-1138.

[3] F.-S. Guo, B. M. Day, Y.-C. Chen, M.-L. Tong, A. Mansikkamäki, R. A. Layfield, *Science* **2018**, *362*, 1400-1403.

[4] aJ. F. Gonzalez, F. Pointillart, O. Cador, *Inorganic Chemistry Frontiers* **2019**, *6*, 1081-1086; bJ. Flores Gonzalez, V. Montigaud, V. Dorcet, K. Bernot, B. Le Guennic, F. Pointillart, O. Cador, *Chemistry–A European Journal* **2021**, *27*, 10160-10168; cJ. Flores Gonzalez, H. Douib, B. Le Guennic, F. Pointillart, O. Cador, *Inorganic chemistry* **2021**, *60*, 540-544.

[5] aP. Evans, D. Reta, G. F. Whitehead, N. F. Chilton, D. P. Mills, *Journal of the American Chemical Society* **2019**, *141*, 19935-19940; bJ. G. Kragskow, J. Marbey, C. D. Buch, J. Nehrkorn, M. Ozerov, S. Piligkos, S. Hill, N. F. Chilton, *Nature communications* **2022**, *13*, 1-10.

[6] G. Cosquer, F. Pointillart, S. Golhen, O. Cador, L. Ouahab, *Chemistry–A European Journal* **2013**, *19*, 7895-7903.

[7] F. Habib, P.-H. Lin, J. Long, I. Korobkov, W. Wernsdorfer, M. Murugesu, *Journal of the American Chemical Society* **2011**, *133*, 8830-8833.

[8] aS. K. Langley, N. F. Chilton, B. Moubaraki, K. S. Murray, *Chemical Communications* **2013**, *49*, 6965-6967; bS. K. Langley, N. F. Chilton, L. Ungur, B. Moubaraki, L. F. Chibotaru, K. S. Murray, *Inorganic chemistry* **2012**, *51*, 11873-11881; cJ.-L. Liu, Y.-C. Chen, Y.-Z. Zheng, W.-Q. Lin, L. Ungur, W. Wernsdorfer, L. F. Chibotaru, M.-L. Tong, *Chemical science* **2013**, *4*, 3310-3316; dX. Lü, W. Bi, W. Chai, J. Song, J. Meng, W.-Y. Wong, W.-K. Wong, R. A. Jones, *New Journal of Chemistry* **2008**, *32*, 127-131.

[9] aA.-L. Boulkedid, J. Long, C. Beghidja, Y. Guari, A. Beghidja, J. Larionova, *Dalton Transactions* **2018**, *47*, 1402-1406; bJ. Long, E. Mamontova, V. Freitas, D. Luneau, V. Vieru, L. F. Chibotaru, R. A. Ferreira, G. Félix, Y. Guari, L. D. Carlos, *RSC advances* **2016**, *6*, 108810-108818; cJ. Long, R. Vallat, R. A. Ferreira, L. D. Carlos, F. A. A. Paz, Y. Guari, J. Larionova, *Chemical Communications* **2012**, *48*, 9974-9976; dA. Upadhyay, C. Das, S. Vaidya, S. K. Singh, T. Gupta, R. Mondol, S. K. Langley, K. S. Murray, G. Rajaraman, M. Shanmugam, *Chemistry–A European Journal* **2017**, *23*, 4903-4916; eA. Upadhyay, S. K. Singh, C. Das, R. Mondol, S. K. Langley, K. S. Murray, G. Rajaraman, M. Shanmugam, *Chemical Communications* **2014**, *50*, 8838-8841.

[10] W.-B. Sun, P.-F. Yan, S.-D. Jiang, B.-W. Wang, Y.-Q. Zhang, H.-F. Li, P. Chen, Z.-M. Wang, S. Gao, *Chemical science* **2016**, *7*, 684-691.

[11] aA. Gnach, A. Bednarkiewicz, *Nano Today* **2012**, *7*, 532-563; bZ. S. Al-Farsi, A. Al-Rashdi, N. K. Al-Rasbi, *Polyhedron* **2016**, *117*, 552-560; cJ.-C. G. Bünzli, C. Piguet, *Chemical Society Reviews* **2005**, *34*, 1048-1077; dB. Lefeuvre, C. A. Mattei, J. F. Gonzalez, F. Gendron, V. Dorcet, F. Riobé, C. Lalli, B. Le Guennic, O. Cador, O. Maury, *Chemistry–A European Journal* **2021**, *27*, 7362-7366; eM. Atzori, K. Dhbaibi, H. Douib, M. Grasser, V. Dorcet, I. Breslavetz, K. Paillot, O. Cador, G. L. Rikken, B. Le Guennic, *Journal of the American Chemical Society* **2021**, *143*, 2671-2675; fJ.-C. G. Buenzli, *Coordination Chemistry Reviews* **2015**, *293*, 19-47.

[12] J. V. Vleck, *Journal of physical chemistry* **1937**, *41*, 67-80.

[13] aJ. Bünzli, S. Comby, A. Chauvin, C. Vandevyver, *Acc. Chem. Res* **2006**, *39*, 53; bA. P. F. D'Aléo, *Coord. Chem. Rev* **2012**, *256*, 1604-1620; cS. V. Eliseeva, J.-C. G. Bünzli, *Chemical Society Reviews* **2010**, *39*, 189-227; dD. Parker, *Chemical Society Reviews* **2004**, *33*, 156-165.

[14] aF. Z. C. Fellah, J.-P. Costes, C. Duhayon, L. Vendier, *Polyhedron* **2016**, *111*, 101-108; bF. Z. C. Fellah, J.-P. Costes, F. Dahan, C. Duhayon, J.-P. Tuchagues, *Polyhedron* **2007**, *26*, 4209-4215.

[15] aJ. Long, J. Rouquette, J. M. Thibaud, R. A. Ferreira, L. D. Carlos, B. Donnadieu, V. Vieru, L. F. Chibotaru, L. Konczewicz, J. Haines, *Angewandte Chemie International Edition* **2015**, *54*, 2236-2240; bT. D. Pasatoiu, C. Tiseanu, A. M. Madalan, B. Jurca, C. Duhayon, J. P. Sutter, M. Andruh, *Inorganic chemistry* **2011**, *50*, 5879-5889; cR.-X. Hu, J. Yang, X. Chen, X. Zhang, M.-B. Zhang, *Inorganica Chimica Acta* **2018**, *482*, 702-708.

[16] aC.-M. Liu, D.-Q. Zhang, J.-B. Su, Y.-Q. Zhang, D.-B. Zhu, *Inorganic chemistry* **2018**, *57*, 11077-11086; bW.-K. Wong, X. Yang, R. A. Jones, J. H. Rivers, V. Lynch, W.-K. Lo, D. Xiao, M. M. Oye, A. L. Holmes, *Inorganic chemistry* **2006**, *45*, 4340-4345; cF. Z. C. Fellah, J.-P. Costes, F. Dahan, C. Duhayon, G. Novitchi, J.-P. Tuchagues, L. Vendier, *Inorganic chemistry* **2008**, *47*, 6444-6451.

[17] aM. Andruh, *Chemical Communications* **2011**, *47*, 3025-3042; bK. Griffiths, J. Mayans, M. A. Shipman, G. J. Tizzard, S. J. Coles, B. A. Blight, A. Escuer, G. E. Kostakis, *Crystal Growth & Design* **2017**, *17*, 1524-1538; cH.-S. Wang, K. Zhang, Y. Song, Z.-Q. Pan, *Inorganica Chimica Acta* **2021**, *521*, 120318.

[18] J. F. Gonzalez, B. Lefeuvre, B. Degraeve, O. Cador, F. Pointillart, *Dalton Transactions* **2021**, *50*, 11466-11471.

[19] aT. D. Pasatoiu, A. M. Madalan, M. U. Kumke, C. Tiseanu, M. Andruh, *Inorganic chemistry* **2010**, *49*, 2310-2315; bM. Dolai, M. Ali, J. Titiš, R. Boča, *Dalton Transactions* **2015**, *44*, 13242-13249.

[20] W. Bi, T. Wei, X. Lü, Y. Hui, J. Song, S. Zhao, W.-K. Wong, R. A. Jones, *New Journal of Chemistry* **2009**, *33*, 2326-2334.

[21] aT. Miao, Z. Zhang, W. Feng, P. Su, H. Feng, X. Lü, D. Fan, W.-K. Wong, R. A. Jones, C. Su, *Spectrochimica Acta Part A: Molecular and Biomolecular Spectroscopy* **2014**, *132*, 205-214; bJ. P. Costes, S. Titos - Padilla, I. Oyarzabal, T. Gupta, C. Duhayon, G. Rajaraman, E. Colacio, *Chemistry–A European Journal* **2015**, *21*, 15785-15796.

[22] aA. Elmali, C. Zeyrek, Y. Elerman, *Journal of molecular structure* **2004**, *693*, 225-234; bY. Lan, G. Novitchi, R. Clérac, J.-K. Tang, N. Madhu, I. J. Hewitt, C. E. Anson, S. Brooker, A. K. Powell, *Dalton Transactions* **2009**, 1721-1727.

[23] aF. Z. C. Fellah, S. Boulefred, A. C. Fellah, B. El Rez, C. Duhayon, J.-P. Sutter, *Inorganica Chimica Acta* **2016**, *439*, 24-29; bM. Dolai, T. Mistri, A. Panja, M. Ali, *Inorganica Chimica Acta* **2013**, *399*, 95-104.

[24] B. Miroslaw, B. Cristóvão, Z. Hnatejko, *Molecules* **2018**, *23*, 1761.

[25] M. Llunell, D. Casanova, J. Cirera, P. Alemany, S. Alvarez, *Program for the Stereochemical Analysis of Molecular Fragments by Means of Continuous Shape Measures and Associated Tools* **2010**.

[26] aM. Maity, M. C. Majee, S. Kundu, S. K. Samanta, E. C. Sañudo, S. Ghosh, M. Chaudhury, *Inorganic chemistry* **2015**, *54*, 9715-9726; bN. Dwivedi, S. K. Panja, A. Verma, T. Takaya, K. Iwata, S. S. Sunkari, S. Saha, *Journal of Luminescence* **2017**, *192*, 156-165.

[27] A. Abdallah, M. Puget, C. Daiguebonne, Y. Suffren, G. Calvez, K. Bernot, O. Guillou, *CrystEngComm* **2020**, *22*.

[28] W.-K. Dong, J.-C. Ma, L.-C. Zhu, Y.-X. Sun, S. F. Akogun, Y. Zhang, *Crystal Growth & Design* **2016**, *16*, 6903-6914.

[29] O. Kahn, *Molecular Magnetisme*, VCH, Weinhem, **1993**.

[30] A. Abragam, B. Bleaney, *Electron paramagnetic resonance of transition ions*, Oxford University Press, **2012**.

[31] A. Singh, K. Shrivastava, *physica status solidi (b)* **1979**, *95*, 273-277.

[32] K. N. Shirivastava, *Phys. Status Solidi B* **1983**, *177*, 437.

[33] F. Pointillart, K. Bernot, S. Golhen, B. Le Guennic, T. Guizouarn, L. Ouahab, O. Cador, *Angewandte Chemie* **2015**, *127*, 1524-1527.

[34] F. Pointillart, J. F. Gonzalez, V. Montigaud, L. Tesi, V. Cherkasov, B. Le Guennic, O. Cador, L. Ouahab, R. Sessoli, V. Kuropatov, *Inorganic Chemistry Frontiers* **2020**, *7*, 2322-2334.

[35] P.-E. Car, M. Perfetti, M. Mannini, A. Favre, A. Caneschi, R. Sessoli, *Chemical Communications* **2011**, *47*, 3751-3753.

[36] M. Maeda, S. Hino, K. Yamashita, Y. Kataoka, M. Nakano, T. Yamamura, T. Kajiwara, *Dalton Transactions* **2012**, *41*, 13640-13648.

[37] aY. Bi, Y. N. Guo, L. Zhao, Y. Guo, S. Y. Lin, S. D. Jiang, J. Tang, B. W. Wang, S. Gao, *Chemistry–A European Journal* **2011**, *17*, 12476-12481; bT. T. Da Cunha, J. Jung, M.-E. Boulon, G. Campo, F. Pointillart, C. L. Pereira, B. Le Guennic, O. Cador, K. Bernot, F. Pineider, *Journal of the American Chemical Society* **2013**, *135*, 16332-16335; cK. Katoh, K. Umetsu, K. Breedlove Brian, M. Yamashita, *Science China Chemistry* **2012**, *55*, 918-925; dF. Tuna, C. A. Smith, M. Bodensteiner, L. Ungur, L. F. Chibotaru, E. J. McInnes, R. E. Winpenny, D. Collison, R. A. Layfield, *Angewandte Chemie* **2012**, *124*, 7082-7086; eM. Waters, F. Moro, I. Krivokapic, J. McMaster, J. van Slageren, *Dalton Transactions* **2012**, *41*, 1128-1130.

[38] G. M. Sheldrick, *Acta Crystallographica Section A: Foundations and Advances* **2015**, *71*, 3-8.

[39] G. M. Sheldrick, *Acta Crystallographica Section C: Structural Chemistry* **2015**, *71*, 3-8.

Entry for the Table of Contents

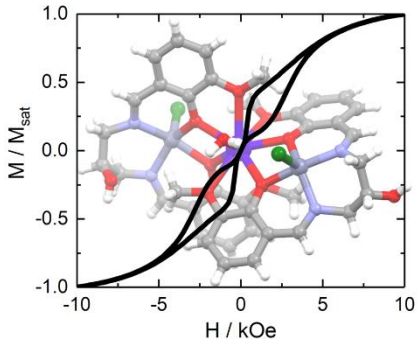

Trinuclear complexes made from Zn(II) Schiff Base metallo-ligand and lanthanide ions highlighted photophysical properties and Single-Molecule Magnet behavior with magnetic bistability up to 5 K.